Nuclear spin temperature and magnetization transport in laser-enhanced NMR of bulk GaAs

Anant K. Paravastu and Jeffrey A. Reimer
Department of Chemical Engineering, University of California at Berkeley, Berkeley, California 94720, USA
(Received 4 February 2004; revised manuscript received 21 September 2004; published 31 January 2005)

Gallium-71 nuclear spin polarizations derived from optical pumping of semi-insulating GaAs were measured through asymmetries in quadrupole-split NMR line shapes. The irradiation time dependences of nuclear polarization and integrated NMR intensity were modeled in terms of spatially inhomogeneous generation of nuclear magnetization coupled with nuclear spin diffusion. Agreement between theory and experiment would require that the spatial extent of the excited electron density be larger than the Bohr radii of electrons confined to hydrogenic defect sites, but smaller than the illuminated region of the sample. The results presented herein place constraints on future modeling of optical nuclear polarization in the solid state, and suggest the importance of both localized and delocalized excited electrons.

DOI: 10.1103/PhysRevB.71.045215 PACS number(s): 76.60.−k, 71.55.Eq, 82.56.Na

I. INTRODUCTION

It is well known that irradiating various direct-gap semiconductors with polarized light can induce enormous enhancements in nuclear spin polarizations relative to thermal equilibrium,[1–5] but the mechanism behind this transfer of angular momentum is not well understood. The lack of a complete model for optically pumped NMR in the solid state is due in part to ambiguities in nuclear magnetic resonance (NMR) and optical measurements performed to date.[3,4,6] One ambiguity concerns the distribution of nuclear spin polarization within the sample, as NMR yields only bulk-averaged signal, and optical schemes for magnetic resonance are biased towards sites of electronic localization. Here, we use a breakdown of the high temperature approximation to measure nuclear spin polarization independently of total NMR intensity. The revealed spatial distributions of optically induced nuclear polarization offer insights into the nuclear polarization process as well as provide constraints for future modeling efforts.

During continuous optical excitation of electrons with polarized photons, growth of GaAs NMR signal may not reveal the microscopic details of angular momentum transfer.[6,7] If electron-nuclear cross relaxation is confined to regions near defect sites ($\sim$100 Å), nuclear spin diffusion could carry magnetization into the bulk and thus polarize the whole crystal.[2,8–10] If, alternatively, delocalized electrons dominate the polarization transfer to nuclei, the effects of nuclear spin diffusion may be negligible as spatial gradients could exist on much larger length scales (laser penetration depths $\sim 1\ \mu$m).[3] In either case, total NMR intensity is expected to grow with time and, in the absence of line shape changes, the NMR spectrum is not necessarily expected to contain information on the source of enhanced nuclear magnetization. The only attempt to experimentally resolve this issue using NMR was stray field imaging of optically pumped nuclear polarization in InP; the resolution in these experiments, however, was insufficient to observe nuclear spin diffusion.[4]

Cross relaxation and spin diffusion both serve to increase the total NMR signal intensity, but they have opposing effects on the bulk-averged nuclear spin polarization. Spin diffusion increases the *number* of polarized nuclei at the expense of the *average* polarization. To elucidate this interplay in optical pumping of bulk GaAs, we employ a method of measuring nuclear polarizations independent of the total NMR intensity.[11] This method exploits asymmetries in the weak quadrupolar splitting of a spin-$\frac{3}{2}$ nucleus (^{71}Ga) in a strained crystal of GaAs. Our results show that the linear growth of laser-enhanced NMR intensity does not always correspond to growth of bulk-averaged nuclear polarizations. In fact, when optical pumping was accomplished by irradiation up to 25 meV below the band gap, growth of average nuclear polarization was highly non-monotonic.

We analyze the detailed time dependence of nuclear spin polarization and NMR intensity derived through irradiation at 1.505 eV using a coupled relaxation-classical diffusion equation. Dimensional analysis shows that highly nonmonotonic growth in average nuclear spin polarization is indicative of spatially inhomogeneous nuclear relaxation without the smoothing effects of nuclear spin diffusion. A quantitative comparison of theory with experimental data shows that the time dependences of NMR signals are consistent with neither defect-bound electrons nor delocalized electrons as the unique source of enhanced nuclear magnetization. The present results suggest the importance of multiple types of excited electrons in polarizing nuclear spins.

II. EXPERIMENTAL

Optically enhanced NMR spectra were collected using the saturation recovery experimental protocol described previously.[3,12] For the present experiments, the sample of semi-insulating GaAs was secured to the sapphire substrate with clamps. The differing thermal expansion coefficients of the substrate and sample holder resulted in strain of the GaAs crystal, as evidenced by a quadrupolar splitting of 4 kHz in the ^{71}Ga (spin-$\frac{3}{2}$) spectra derived from optical pumping (see Fig. 1). Given the modest penetration depth of the pumping irradiation, and the significantly diminished quadrupolar satellite intensity in the thermally polarized (bulk) NMR spectrum (inset, Fig. 1), we conclude that the majority of the

 ©2005 The American Physical Society

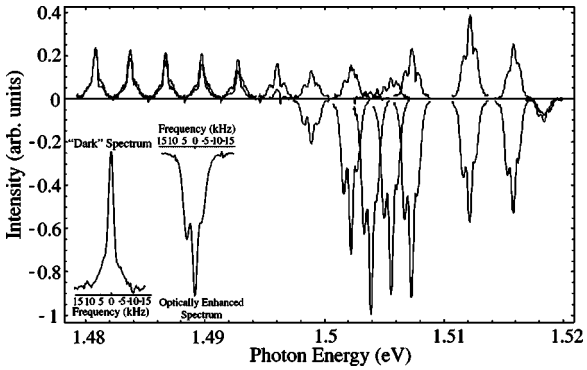

FIG. 1. ^{71}Ga laser-enhanced NMR line shape as a function of photon energy. The NMR spectra are positioned so that the central transitions are aligned with the excitation photon energy on the horizontal axis. Spectra were phase adjusted so that positive peaks indicate net nuclear spin alignment with the external magnetic field. There are two spectra for each photon energy, corresponding irradiation with σ^+ or σ^- circularly polarized light. In all cases, σ^+ light yielded lower or negative intensity. Sample temperature=10 K, laser power=200 mW, laser spot diameter=4 mm, and irradiation time=4 min. Inset: A "dark" spectrum, collected without laser enhancement, and the spectrum obtained through irradiation at 1.505 eV with σ^+ light, both plotted on a frequency scale. Neither spectrum in the inset is drawn to scale.

sample strain was confined to the near-surface region of the GaAs crystal.

For each spectrum, we obtained quadrupolar line shapes by summing 256 successive acquisitions preceded by short pulses (5°). Successive acquisitions were separated in time by more than 5 T_2, and the data were found to be independent of the delay between acquisitions. The laser was on during signal acquisition, and no changes were observed when the laser was blocked prior to signal acquisition. A four-step CYCLOPS phase cycle[13] was necessary in order to obtain reproducible results. Spectral parameters were extracted from nonlinear fits of the free induction decays and were not sensitive to the loss of signal during the probe recovery time (10 μs).

III. QUALITATIVE DESCRIPTION OF RESULTS

A. Dependence of spin temperature on photon energy

Figure 1 shows optical pumping-derived NMR spectra as a function of excitation photon energy. Total NMR intensities varied with photon energy in agreement with previous measurements of unsplit NMR lines.[3] Also shown is the "dark" spectrum, which was acquired for partially thermally relaxed nuclei.[27]

Optically pumped NMR line shapes were split into three peaks due to a 4 kHz quadrupolar splitting induced by crystal strain. The peak in the center was more intense than expected for a quadrupole-split spin-$\frac{3}{2}$ nucleus,[14] indicating that some intensity in the central line was due to nuclei in symmetric environments. At photon energies above 1.495 eV, about 80% of the signal intensity was due to nuclei exhibiting quadrupolar splittings. This percentage was smaller ($\sim$20%–40%) for lower photon energies and in the dark spectrum, suggesting that light with photon energy below 1.495 eV penetrated further into the sample where strain was diminished. The magnitude of the quadrupolar contribution to NMR intensity and the splitting itself showed no dependence on irradiation time.

At photon energies below the band gap (<1.52 eV), quadrupolar line shapes were asymmetric, indicating low spin temperatures.[11] The ratio of satellite intensities is a function of the population differences between corresponding nuclear spin energy levels:[15]

$$\frac{I_{-1/2\rightarrow -3/2}}{I_{3/2\rightarrow 1/2}} = \exp\left(-\frac{2\hbar\gamma_n B_0}{kT_n}\right), \tag{1}$$

where $I_{i\rightarrow j}$ is the intensity of the NMR line corresponding to transitions between the nuclear spin energy levels with quantum numbers i and j, γ_n is the nuclear magnetogyric ratio, B_0 is the external magnetic field, and T_n is the nuclear spin temperature. Knowledge of T_n allows the calculation of the nuclear polarization according to

$$\langle I_z\rangle = \frac{1}{2}\tanh\frac{\hbar\gamma_n B_0}{2kT_n} + \tanh\frac{\hbar\gamma_n B_0}{kT_n}. \tag{2}$$

Equations (1) and (2) are valid only if the nuclear spin system can be described by a single spin temperature, T_n, and preclude potential spatial inhomogeneities in nuclear magnetization. Because the left-hand side of Eq. (1) is determined from bulk-averaged experimental data, we define the "bulk-averaged" quantities $\overline{T_n}$ and $\overline{\langle I_z\rangle}$ as those values extracted from Eqs. (1) and (2) and the satellite intensities. These values could be the result of averaging over spatially inhomogeneous distributions of magnetization.

At fixed photon energy, changes to photon polarization and laser power resulted in systematic changes to the measured asymmetries and NMR intensities, confirming that both quantities are related through the nuclear spin polarization. Asymmetry also inverted when irradiation with opposite photon polarizations caused the NMR intensity to invert, as can be seen clearly, for example, at 1.515 eV in Fig. 1.

When irradiation was above the band gap (>1.52 eV), the quadrupolar line shapes (not shown) were symmetric except at much longer irradiation times (>1 h). The intensities of superband gap optically pumped NMR signals were larger than predicted from satellite assymetry-derived limits on the spin temperatures. When compared to subband gap irradiation, superband gap NMR enhancements were therefore due to more nuclear spins with lower polarizations.

B. Irradiation time dependence of signal intensity and spin polarization at a photon energy of 1.505 eV

The present results demonstrate that optically pumped NMR intensity and nuclear spin polarization are related, but distinct, quantities. Measuring the ^{71}Ga quadrupolar line shape as a function of irradiation time revealed highly nonmonotonic growth of nuclear polarizations despite linear growth in the NMR signal intensity for irradiation at photon energies up to 25 meV below the band gap.

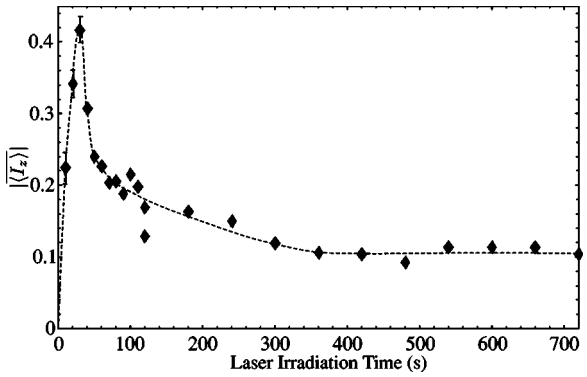

FIG. 2. Growth of $|\overline{\langle I_z \rangle}|$ (defined in text) as a function of irradiation time. Sample temperature = 10 K, photon energy = 1.505 eV, laser power = 200 mW, and photon polarization = σ^+. The actual spin polarizations were negative for irradiation with σ^+ polarized light. Error bars are 2 standard deviations, estimated based on the quality of fits of the free induction decays (Ref. 16). Scatter beyond the error bars may be due to fluctuations in the laser power. The dashed line is a guide to the eye.

Figure 2 shows the irradiation time dependence of $|\overline{\langle I_z \rangle}|$ for a photon energy of 1.505 eV and σ^+ polarization, and Fig. 3 shows that the total integrated NMR intensity obtained in the same experiments was a linear function of time. The satellite intensity-derived $|\overline{\langle I_z \rangle}|$ increased rapidly for the first 30 s of irradiation and then started to decrease. For irradiation times above 30 s, the simultaneous drop in $|\overline{\langle I_z \rangle}|$ and growth in total signal intensity indicates the slowly growing contribution to NMR signal from large numbers of weakly polarized nuclear spins at the expense of the average polarization. Since the observed total and satellite intensities ultimately derive from cross-relaxation between electrons and nuclei, this result implies a spatially inhomogeneous polarization transfer process. Therefore, any model for present phenomena must account for both spatial and temporal changes to the nuclear spin system with increasing irradiation time.

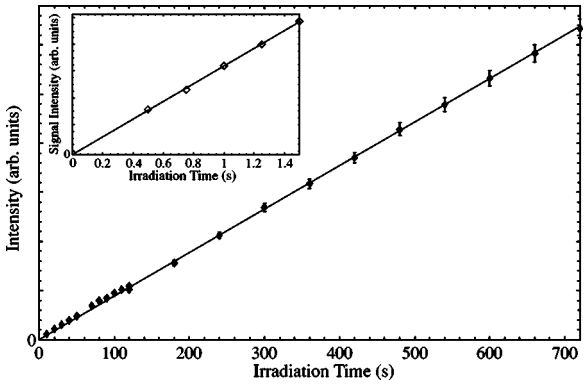

FIG. 3. Change of absolute NMR signal intensity with increasing irradiation time between saturation and detection of magnetization. Sample temperature = 10 K, photon energy = 1.505 eV, laser power = 200 mW, and photon polarization = σ^+. The actual peaks were negative in intensity for irradiation with σ^+ polarized light. Inset: previously published (Ref. 3) early time dependence of laser-enhanced signal intensity at 1.505 eV. Although the previous data did not correspond to quadrupole-split line shapes, they were collected under similar conditions to the present results and demonstrate that the linear time dependence of NMR intensity persists to earlier times.

Since previous measurements of the optically pumped NMR line shape in bulk GaAs have revealed little information on the microscopic dynamics of nuclear magnetization within the sample,[3] the data in Fig. 2 offer an opportunity to assess the geometry and length scales of spatial inhomogeneities in nuclear relaxation rates. The prevailing model in the literature for optical polarization of bulk nuclear spins in GaAs predicts spatial inhomogeneities due to trapping of excited electrons at defect sites; electron-induced nuclear relaxation rates are therefore anticipated to vary over the length scale of the Bohr radius of a donor-bound electron ($\sim$100 Å).[2,9,10] This model was motivated by NMR line shapes detected optically for GaAs at lower magnetic field (0.6 T).[9] It was subsequently argued that the model is applicable to high-field optically pumped NMR through sample-in-coil detection, because of the large NMR enhancements observed for irradiation below the band gap.[1,2] If defect sites are dilute within the sample, this mechanism would predict spherical symmetry for the spin diffusion around hydrogenic defect sites at short times. As nuclei within defect sites reach their steady-state polarizations, $|\overline{\langle I_z \rangle}|$ might be expected to decrease with the increasing contribution to intensity from nuclei farther away.

Alternatively, it has also been suggested that optical NMR enhancements are due to direct interactions between bulk nuclei and delocalized excited electrons.[3] Under this mechanism, spatial inhomogeneities in nuclear relaxation would be expected to exist on the length scale of light penetration into the sample ($\sim 1\ \mu$m), and the geometry of spin diffusion would be one-dimensional in the direction perpendicular to the illuminated surface. In this case, the nonmonotonic temporal dependence of $|\overline{\langle I_z \rangle}|$ may be due to the fact that near-surface nuclear spins would reach their steady-state spin polarizations more rapidly than spins further into the sample.

IV. QUANTITATIVE ANALYSIS OF RESULTS

In the next few sections, we test the previous hypotheses through microscopic analysis of nuclear spin relaxation and magnetization transport. We attempt to fit the data in Figs. 2 and 3 to solutions of the well-known spin diffusion equation,[2,9,17–19]

$$\frac{\partial \langle I_z \rangle}{\partial t} = \frac{1}{T_1(\vec{r})}(\langle I_z \rangle_\infty - \langle I_z \rangle) + D\nabla^2 \langle I_z \rangle, \tag{3}$$

where t is the irradiation time, $\langle I_z \rangle_\infty$ is the limiting spin polarization induced by the Overhauser effect, $1/T_1(\vec{r})$ is the local relaxation rate through direct interaction with electron density, and D is the nuclear spin diffusivity. The driving force for development of spatial inhomogeneities in $\langle I_z \rangle$ is the spatial dependence of $1/T_1(\vec{r})$. Regardless of geometry, the initial condition of Eq. (3) is $\langle I_z \rangle = 0$ at $t = 0$, as ensured by saturation of NMR signal at the beginning of the NMR pulse sequence.

Solutions of Eq. (3) can be compared to experimentally measured data for $\langle I_z \rangle$ using the following spin temperature arguments. With the assumption that spin temperature is always well defined throughout the sample, Eq. (2) establishes a relationship between the spatial dependences of spin polarization and spin temperature ($\langle I_z \rangle$ and T_n, respectively). The contribution from a given region of the sample to the intensity of an NMR line is directly proportional to local nuclear spin population (p_i) differences, which are determined solely by the spin temperature. Therefore the bulk-averaged NMR signal intensity and the ratio of quadrupolar satellite intensities are given by[14]

$$\text{NMR Intensity} \propto \int \left(\frac{3}{2}(p_{3/2} - p_{1/2}) + 2(p_{1/2} - p_{-1/2}) + \frac{3}{2}(p_{-1/2} - p_{3/2}) \right) dV = \int \langle I_z \rangle dV \quad (4)$$

and

$$\frac{I_{-1/2 \rightarrow -3/2}}{I_{3/2 \rightarrow 1/2}} = \frac{\int (p_{-3/2} - p_{-1/2}) dV}{\int (p_{1/2} - p_{3/2}) dV}, \quad (5)$$

where the local populations p_i are determined by Boltzmann statistics:

$$p_i = \frac{\exp\left(\frac{i\hbar \gamma_n B_0}{kT_n} \right)}{\sum_{j=-3/2}^{3/2} \exp\left(\frac{j\hbar \gamma_n B_0}{kT_n} \right)}. \quad (6)$$

Finally, the bulk-averged nuclear spin temperature, $\overline{T_n}$, can be calculated from the quadrupolar satellite intensity ratio using Eq. (1) and input to Eq. (2) to yield an estimate for the bulk-averaged nuclear spin polarization, $\overline{\langle I_z \rangle}$.

One may question the validity of the present analysis through the observation that the NMR line shapes were not 100% quadrupolar in nature. There was a significant ($\sim$20%) contribution to signal from nuclei in symmetric environments, and spin diffusion may have transferred polarization between strained and unstrained regions of the sample. Since the ratio of the quadrupolar-perturbed signal to the unperturbed signal was unaffected by changing irradiation time, we conclude that transport of nuclear magnetization between these regions was unlikely.

A. Spin transport in a spherically symmetric geometry

To model the process of coupled nuclear relaxation and spin diffusion from dilute donor impurity sites, we specify the origin of our coordinate system to be the center of a single defect site. The predictions of this model are representative of the bulk signal as long as the diffusion profiles from neighboring defect sites do not interact, and there are no other relaxation mechanisms in the bulk of the crystal.

The electron density, and therefore the distribution of nuclear relaxation rates, is expected to be spherically symmetric:[9]

$$\frac{1}{T_1(r)} = \frac{1}{T_{1,0}} f(r), \quad (7)$$

where $T_{1,0}$ is the nuclear relaxation time at the origin and $f(r)$ is a normalized function that describes the shape of the distribution of relaxation rates. If the bound electronic wave functions are hydrogenic, the ground electronic state would resemble an *s* orbital,[9]

$$|\psi(r)|^2 \propto \exp(-2r/a), \quad (8)$$

where a is the Bohr radius of the donor-bound electronic wave function. For nuclei in the vicinity of the bound electron, the dominant interaction is Fermi contact

$$H_{\text{fc}} = A_{\text{fc}} \vec{S} \cdot \vec{I}, \quad (9)$$

where A_{fc} is a hyperfine coupling constant that is proportional to $|\psi(r)|^2$. The local relaxation rate is proportional to A_{fc}^2, leading to a spatial dependence for the relaxation rate of the form[9]

$$f(r) = \exp(-4r/a). \quad (10)$$

Equations (3), (7), and (10) are most easily analyzed in nondimensional form. We scale all variables by their characteristic dimensions:

$$\widetilde{\langle I_z \rangle} \equiv \frac{\langle I_z \rangle - \langle I_z \rangle_\infty}{\langle I_z \rangle_\infty},$$

$$\tilde{t} \equiv \frac{t}{T_{1,0}},$$

$$\tilde{r} \equiv \frac{r}{a}.$$

Equation (3), in nondimensional form, becomes

$$\frac{\partial \widetilde{\langle I_z \rangle}}{\partial \tilde{t}} = \underbrace{\frac{DT_{1,0}}{a^2}}_{\equiv \zeta} \nabla^2 \widetilde{\langle I_z \rangle} - \tilde{f}(\tilde{r}) \widetilde{\langle I_z \rangle}, \quad (11)$$

where the nondimensional shape function $\tilde{f}(\tilde{r})$ is given by

$$\tilde{f}(\tilde{r}) = \exp(-4\tilde{r}). \quad (12)$$

The new temporal limits are

$$\widetilde{\langle I_z \rangle}(\tilde{r}, 0) = -1, \quad (13)$$

$$\lim_{t \rightarrow \infty} \widetilde{\langle I_z \rangle}(\tilde{r}, \tilde{t}) = 0. \quad (14)$$

Equation (11) can fully capture the relaxation-diffusion problem with a single parameter, ζ, rather than the four parameters (D, $\langle I_z \rangle_\infty$, $T_{1,0}$, and a) necessary for evaluation of Eq. (3). Furthermore, ζ has physical significance, as it is the ratio of the spin diffusion rate (D/a^2) to the rate of signal generation at the origin ($1/T_{1,0}$). We have numerically solved Eq. (11) using the method of finite elements in Matlab for different values of ζ. The results of these numerical calculations are the basis of the present discussion.

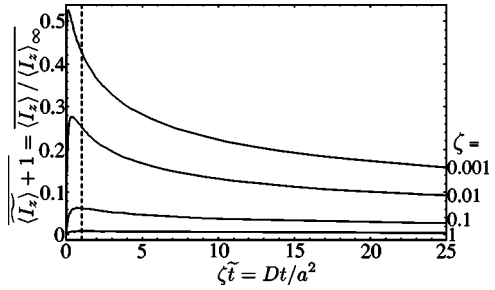

FIG. 4. Theoretical growth of average nuclear spin polarization in nondimensional form for different values of ζ, assuming a spherical geometry for nuclear relaxation and spin diffusion. The horizontal scale, $\zeta\tilde{t}$, corresponds to the square of the ratio of the penetration length of spin diffusion ($\sqrt{Dt}$) to the characteristic length of the relaxation rate distribution (a). The vertical dashed line at $Dt/a^2 = 1$ indicates the time past which spin diffusion has transferred polarization outside Bohr radius of the defect site. The vertical axis is the average spin polarization relative to its maximum possible value.

We aim to compare numerical evaluations of Eq. (11) to the data in Figs. 2 and 3. The key points of comparison between the model and the data are the following.

(1) $|\overline{\langle I_z\rangle}|$ initially increased with time, reached a maximum value, and then decreased with time, as in Fig. 2.

(2) The magnitude of the NMR signal intensity increased linearly with time, as in Fig. 3.

(3) No hyperfine shift or broadening of the NMR spectrum was observed.

Figure 4 shows the theoretical growth of spin polarization as a function of time, obtained by solving Eq. (11), and Fig. 5 shows the corresponding theoretical growth in signal intensity. In the next section, the former will be compared to satellite intensity-derived polarizations, and the latter to the integrated signal intensitites. Before quantitative comparison of theoretical results to experimental data, we briefly discuss the theoretical curves in nondimensional form so that general trends may be described without consideration of specific parameter estimates.

For the full range of ζ values in Fig. 4, the peak in the average nuclear spin polarization occurred when signal was primarily due to nuclei within the Bohr radius of the electronic wave function ($\sqrt{Dt} < a$); the specific time at which this maximum occurs is affected by the interplay between growth of magnetization inside the defect site and transport of magnetization away. Figure 4 indicates that nonmonotonic

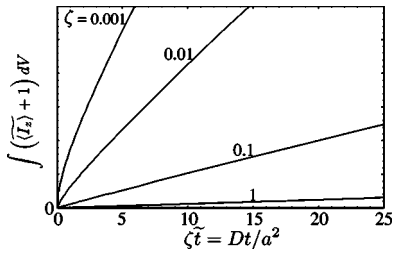

FIG. 5. Theoretical growth of total intensity in nondimensional form for different values of ζ and a rectangular geometry for nuclear spin relaxation and spin diffusion.

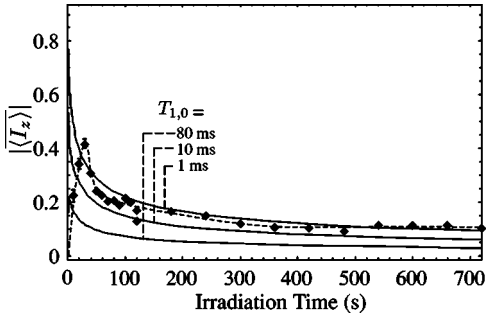

FIG. 6. Data from Fig. 2 plotted against predictions from solutions of Eq. (3), assuming a spherical geometry. The parameters used in the theoretical curves were $a = 100$ Å, $D = 3000$ Å^2/s, $\langle I_z\rangle_\infty = -1.25$, and the $T_{1,0}$ values marked on the graph. The dashed line is a smooth curve through the data points, provided as a guide to the eye.

growth in $|\overline{\langle I_z\rangle}|$ is possible in this geometry for small values of ζ, i.e., when the polarization process is diffusion limited (by small diffusivity, fast relaxation, or large Bohr radius). Diffusion limitation is also required in order to achieve the experimental magnitudes of $|\overline{\langle I_z\rangle}|$ reported in Fig. 2.

While the theoretical curves in Fig. 4 point towards a diffusion limitation (small ζ), two consequences of a diffusion limitation contradict experimental observations. First, small ζ results in nonlinear growth in signal intensity (Fig. 5). Second, the period when $|\overline{\langle I_z\rangle}|$ increases with irradiation time corresponds to signal primarily from nuclear spins within the Bohr radius of the defect site; these spins would be expected to exhibit detectable hyperfine shifts. The experimental short irradiation time ($\sim$1 s) behavior of laser-enhanced NMR indicates linear growth of intensity and no detectable shift or broadening of the spectrum. In the next section, we compare the numerical predictions of the relaxation-diffusion equation in dimensional form [Eq. (3)] with the data in order to quantify these discrepancies.

B. Comparison of theory and experiment for spherically symmetric spin diffusion

The Bohr radius of a typical defect site has been measured to be approximately $a \sim 100$ Å (Ref. 9). For the ^{71}Ga spin diffusivity, we use the value $D \sim 3000$ Å^2/s (Refs. 9 and 10). With these values, $\sqrt{Dt}$ is equal to a at $t = 3$ s, making early times—when signal is ostensibly due to nuclei near defect sites—experimentally accessible. This time is much shorter than irradiation time that yielded the largest value of $|\overline{\langle I_z\rangle}|$ in Fig. 2, making it impossible for Eq. (3) to agree with the first 30 s of the measured time dependence of $\overline{\langle I_z\rangle}$, at least for the specified values of a and D.

Figure 6 shows the measured change of $\overline{\langle I_z\rangle}$ with time plotted against numerical solutions of Eq. (3) for a series of possible $T_{1,0}$ values. In order to best fit the data, the limiting spin polarization, $\langle I_z\rangle_\infty$, was assumed to be at its maximum possible magnitude ($\langle I_z\rangle_\infty = -1.25$).[28] Figure 6 indicates that relaxation must be fast within the defect site ($T_{1,0} \sim 1$ ms, top curve, Fig. 6) in order for Eq. (3) to predict the high ob-

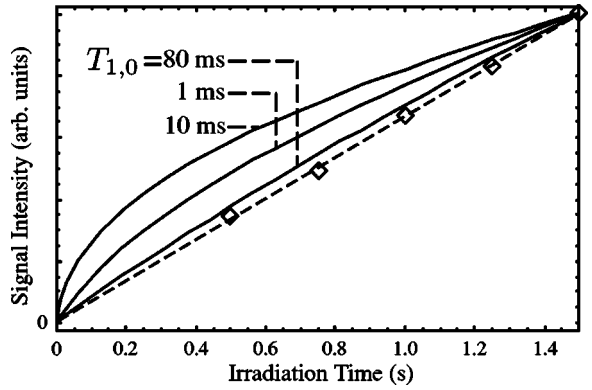

FIG. 7. Data from Fig. 3 plotted against predictions from solutions of Eq. (3), assuming a spherical geometry. The parameters used in the theoretical curves were $a=100$ Å, $D=3000$ Å^2/s, $\langle I_z\rangle_\infty=-1.25$, and the $T_{1,0}$ values marked on the graph. Because the intensity scale is arbitrary, the theoretical curves were scaled to meet at 1.5 s. The dashed line is a straight line from the origin through the data, representing signal intensity that is proportional to irradiation time.

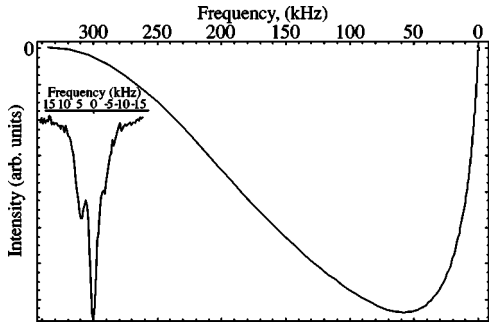

FIG. 8. A sample theoretical NMR line shape, based on hyperfine fields calculated using Eq. (16), and the profile of nuclear magnetization predicted by Eq. (3). The parameters used in this simulation were $t=30$ s, $D=3000$ cm^2/s, $\langle I_z\rangle_\infty=-1.25$, $T_{1,0}=80$ ms, $a=100$ Å, and $\langle S_z\rangle=0.056$. The factor $FA_{\rm fc}$ required in Eq. (16) was calculated with Eq. (15), assuming $\gamma_e=\omega_e-\omega_n$. Inset: an experimental NMR spectrum, for $t=30$ s, and irradiation at 1.505 eV with σ^+ light.

served nuclear spin polarizations. This relaxation time is much shorter than the value of 80 ms reported from optical measurements at lower magnetic field.[9] As anticipated, no value of $T_{1,0}$ is consistent with the observed early rise in $|\overline{\langle I_z\rangle}|$ that persisted to 30 s.

Figure 7 compares the early-time signal growth predicted by Eq. (3) with the measured linear growth of signal intensity near 1 s (inset, Fig. 3). This measured short time dependence indicatesthat the relaxation times necessary to fit the measured values of $|\overline{\langle I_z\rangle}|$ (Fig. 6) would yield nonlinear generation of signal (Fig. 7). Therefore, Eq. (3) cannot simultaneously predict the time dependences of $\overline{\langle I_z\rangle}$ and signal intensity under the present assumptions.

With the model for nuclear polarization via localized excited electrons, knowledge of $T_{1,0}$ allows the calculation of the predicted hyperfine-broadened NMR line shapes.[10] The hyperfine coupling constant can be estimated according to

$$\frac{1}{T_{1,0}}=\frac{F^2A_{\rm fc}^2}{2}\frac{\gamma_e}{\gamma_e^2+(\omega_e-\omega_n)^2}, \tag{15}$$

where F is the probability of a defect site being occupied by an electron and γ_e is a characteristic frequency of fluctuations in the hyperfine field.[2,9,10] The time-average value of the Fermi contact interaction at a given position is

$$\overline{H_{\rm fc}}(r)=FA_{\rm fc}\exp(-2r/a)\langle S_z\rangle, \tag{16}$$

where $\langle S_z\rangle$ is the electron spin polarization. Using Eqs. (15) and (16), the hyperfine broadening of the NMR signal can be predicted from the hyperfine coupling constant and the spatial dependences of nuclear polarization and electron density.[10]

Figure 8 shows a theoretical line shape calculated with parameter choices that minimize predicted hyperfine broadening. Comparison with the experimental line shapes (inset) shows that this mechanism does not contribute to NMR line shapes. It is worth noting that $\langle S_z\rangle$ cannot be arbitrarily small given the large measured magnitudes of $\overline{\langle I_z\rangle}$ and the significant modulation of NMR intensity induced by different light polarizations (see Appendix A).

The broad line shapes estimated for laser-enhanced NMR with polarized light have been predicted previously,[10] but they are not consistent with experiments. Since Eq. (3) predicts that shorter times correspond to signal from nuclei closer to the centers of electron density, more broadening is expected at shorter irradiation times. We have measured no broadening whatsoever at irradiation times as short as 0.5 s for any polarization of light *with or without* shuttering the laser before acquisition. We therefore conclude that the nuclei polarized by laser light do not experience the strong hyperfine fields expected from a highly localized electron-nuclear polarization transfer.

To complete the analysis of optical nuclear polarization through spherically symmetric cross relaxation and spin diffusion, we consider the possibility that the effective Bohr radii of defect-bound electrons in the sample may have been much larger than measured previously,[9] perhaps through defect clustering. Figure 9 shows the data in Fig. 2 plotted against solutions of Eq. (3) derived from values of a chosen so that the maximum value of $\overline{\langle I_z\rangle}$ would occur at an irradiation time near that observed in the data ($\sim$30 s). These curves do not agree quantitatively with the data. Furthermore, Fig. 10 shows the corresponding predicted time dependence of the signal intensity; the nonlinear behavior at longer time scales ($\sim$ minutes) is also inconsistent with experimental data.[3]

In summary, the model invoking electron-nuclear cross relaxation within the Bohr radii of donor-bound electrons and spin diffusion into the bulk is characterized by four parameters: a, D, $T_{1,0}$, and $\langle I_z\rangle_\infty$. The first two parameters can be predicted with reasonable accuracy from previous measurements.[9] Agreement between this model and the magnitudes of bulk-averaged spin polarizations reported in Fig. 2 requires small estimates for $T_{1,0}$ ($\sim$1 ms) and large estimates for $|\langle I_z\rangle_\infty|$ ($\sim$1.25). However, these parameter estimates would lead to predictions of significant hyperfine broadening

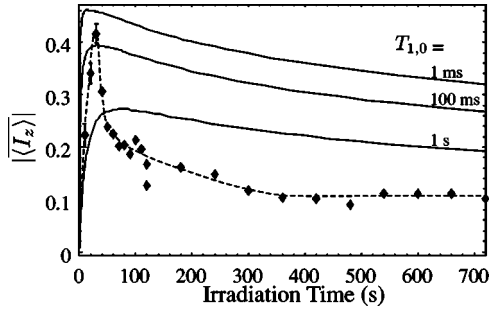

FIG. 9. Data from Fig. 2 plotted against predictions from solutions of Eq. (3), assuming a spherical geometry. The theoretical curves correspond to larger Bohr radii ($a \sim 1000$ Å) than would be expected for single donor-bound electrons or excitons, and were chosen so that the maximum predicted $|\overline{\langle I_z \rangle}|$ would correspond to roughly 30 s of irradiation. $D = 3000$ Å^2/s, $\langle I_z \rangle_\infty = -0.65$, and the $T_{1,0}$ values marked on the graph. The dashed line is a smooth curve through the data points, provided as a guide to the eye.

of the NMR spectrum and nonlinear growth in signal intensity, neither of which was observed experimentally. In addition, no set of reasonable parameter estimates could yield good agreement with the measured time dependence of $\overline{\langle I_z \rangle}$ before 30 s. The data favor distributions of nuclear spin relaxation rates that vary on length scales larger than the Bohr radii of donor-bound electrons, but the data cannot be fit by increasing the effective defect Bohr radii alone.

C. Spin transport in a rectangular geometry

An alternative proposed mechanism for optically pumped NMR in GaAs invokes delocalized excited electrons, such as free excitons, to polarize bulk nuclei.[3] This model was motivated by the temperature dependence of optical NMR enhancements, and the significant enhancements observed for photon energies above the band gap.[3] The spatial dependence of excited electron concentrations would be determined by the drop in light intensity as it penetrates into the surface of GaAs and by the diffusion of mobile carriers during the excited state lifetime. The geometry of nuclear spin diffusion under this model is expected to be one dimensional in the direction parallel to that of light propagation (perpendicular to the sample surface).

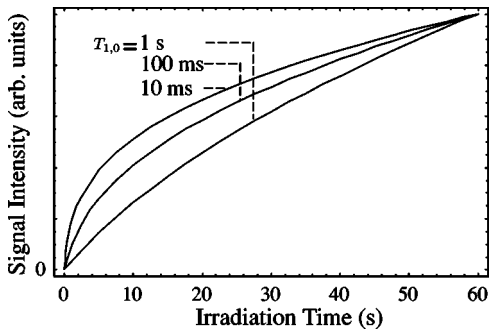

FIG. 10. The theoretical curves for the growth of NMR signal intensity with the parameter estimates from Fig. 9: $a = 1000$ Å, $D = 3000$ Å^2/s, $\langle I_z \rangle_\infty = -0.65$, and the $T_{1,0}$ values marked on the graph.

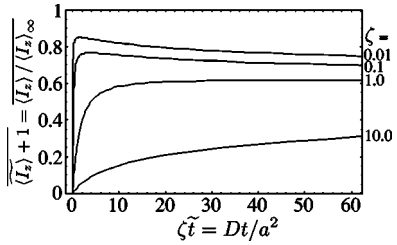

FIG. 11. Theoretical growth of average nuclear spin polarization in nondimensional form for different values of ζ and a rectangular geometry for nuclear spin relaxation and spin diffusion. The horizontal scale, $\zeta\tilde{t}$, corresponded to the square of the ratio of the penetration length of spin diffusion ($\sqrt{Dt}$) to the characteristic length of the relaxation rate distribution (a). The vertical axis is the average spin polarization relative to its maximum possible value.

In this rectangular geometry, the nondimensional diffusion equation [Eq. (11)] remains valid; the relevant spatial coordinate is the distance from the illuminated surface into the bulk, x:

$$\frac{\partial \widetilde{\langle I_z \rangle}}{\partial \tilde{t}} = \zeta \frac{\partial^2 \widetilde{\langle I_z \rangle}}{\partial \tilde{x}^2} - \tilde{f}(\tilde{x}) \widetilde{\langle I_z \rangle}, \tag{17}$$

where $\tilde{x}$ is x/a. The characteristic nuclear spin relaxation time, $T_{1,0}$, is now the nuclear relaxation time at the surface of the crystal where the light intensity is highest. The characteristic length scale, a, is roughly the penetration depth of the light. As before, it is presumed that, given infinite irradiation time, the whole nuclear spin reservoir would be polarized to $\langle I_z \rangle_\infty$. The shape function, $\tilde{f}(\tilde{x})$, is assumed to be a single exponential, since the nuclear relaxation rate is assumed to be directly proportional to the light intensity:

$$\tilde{f}(\tilde{x}) = \exp(-\tilde{x}). \tag{18}$$

Figures 11 and 12 show the calculated dependences of nuclear spin polarization and NMR intensity on irradiation time based on numerical solutions of Eq. (17), calculated using the method of finite differences in Matlab. It can be seen from Fig. 11 that a rectangular geometry for spin diffusion could also lead to a nonmonotonic growth in $\overline{\langle I_z \rangle}$, as was calculated for the spherical geometry (Fig. 4).

Just as with the spherical geometry, nonmonotonic growth of $\overline{\langle I_z \rangle}$ corresponds to small values of ζ and therefore diffu-

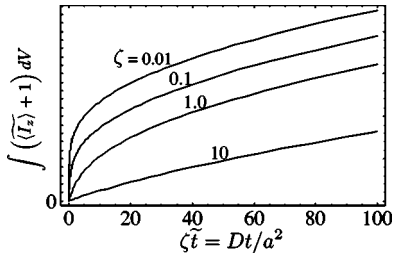

FIG. 12. Theoretical growth of total intensity in nondimensional form for different values of ζ and a rectangular geometry for nuclear spin relaxation and spin diffusion.

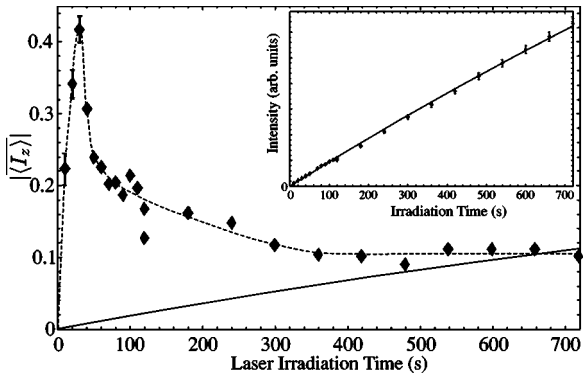

FIG. 13. Theoretical growth $|\overline{\langle I_z \rangle}|$ as a function of irradiation time for a rectangular geometry of nuclear relaxation and spin diffusion (solid line), plotted against data from Fig. 2. The model invoking delocalized electrons for nuclear polarization is capable of predicting the magnitudes of observed nuclear polarizations for long irradiation times. Parameter estimates used for the theoretical (solid) curve: $a=1$ μm, $D=3000$ Å^2/s, $T_{1,0}=1667$ s, $\langle I_z \rangle_\infty = 0.6$. Inset: predicted time dependence of NMR intensity (solid line) for these parameter estimates, plotted with data from Fig. 3.

sion limitation. The requirement of small values of ζ is again at odds with the observation of a linear dependence of total signal intensity on irradiation time (Fig. 12).

D. Comparison of theory and experiment for spin diffusion in a rectangular geometry

The assumption of complete delocalization of excited electrons implies that a is on the order of the light penetration depth (~ 1 μm).[3,20] The nuclear spin diffusivity, D, is not expected to vary with the geometry of spin diffusion; this parameter estimate therefore remains 3000 Å^2/s. With a and D thus specified, a single unit on the horizontal axis of Fig. 11 corresponds to an irradiation time t of $a^2/D \sim 10^4$ s. It is therefore clear that the present model could not predict a peak in $\overline{\langle I_z \rangle}$ for irradiation times as early as 30 s. This discrepancy could not be remedied by reducing estimates for ζ below 0.01, because this reduction would require estimates for $T_{1,0}$ that are below 300 s. Such low estimates for $T_{1,0}$ would correspond to highly nonlinear growth in NMR signal intensity (for irradiation times on the order of $T_{1,0}$; Fig. 12), whichwas not observed experimentally (Fig. 3).

We comment that, while the model invoking delocalized electrons can not reasonably predict the experimental time dependence of $|\overline{\langle I_z \rangle}|$, the observed magnitudes of nuclear polarizations for long irradiation times could be predicted for reasonable parameter estimates, as shown in Fig. 13. We therefore do not rule out the potential importance of electron-nuclear cross relaxation in the bulk of the crystal.

V. DISCUSSION

Irradiation of GaAs with light at photon energy 1.505 eV yields linear growth of optically pumped NMR intensity and nonmonotonic growth in bulk-averaged nuclear spin polarization ($\overline{\langle I_z \rangle}$). The latter result indicates that nuclear spin relaxation rates are spatially inhomogeneous within the sample. We have attempted to model the temporal dependence of $\overline{\langle I_z \rangle}$ by considering two extremes in the degree of electronic localization, i.e., electrons localized to hydrogenic defect sites or delocalized over the illuminated region. In both theoretical cases, highly nonmonotonic growth in $\overline{\langle I_z \rangle}$ corresponded to diffusion limitation, suggesting that the experimental distribution of optically pumped nuclear spin polarization is not affected strongly by nuclear spin diffusion. However, our inability to model the data quantitatively raises questions as to the identity and nature of the excited electrons that transfer angular momentum to the nuclear spin system.

Reasonable hydrogenic-defect estimates for a and D could not allow Eq. (3) to predict simultaneously the nonmonotonic time dependence of $|\overline{\langle I_z \rangle}|$, the linear growth in signal intensity at experimental time scales (between 0.5 and 700 s), and the lack of hyperfine broadening of the NMR spectra. The experimental time dependence of $|\overline{\langle I_z \rangle}|$ suggests the importance of electronic localization, but the linear growth of NMR intensity and the lack of hyperfine broadening indicate that the NMR signal emanates from nuclei distributed over bulklike length scales. The positive growth in $|\overline{\langle I_z \rangle}|$ for the first 30 s indicates that the characteristic length scale, a, is much larger than the Bohr radii of donor impurity sites.[9] Such a large value of a might suggest clustering of impurity sites or weak trapping of mobile excitons. Increasing a alone, however, did not yield good quantitative agreement with the measured growth of $\overline{\langle I_z \rangle}$, and the best-fit values of $T_{1,0}$ (longest) led to predictions of nonlinear growth at longer time scales (~ 1 min). Electronic localization could play a role in optically pumped NMR enhancements, yet we have not identified the nature of this localization.

Agreement between theory and experiment was not improved by assuming complete delocalization of excited electrons. While inhomogeneities in light intensity caused by the finite penetration depth of the light could lead to nonmonotonic growth in $\overline{\langle I_z \rangle}$, our calculations in the rectangular geometry indicate that maximum $\overline{\langle I_z \rangle}$ would be observed at irradiation times much longer than the experimental value of 30 s. Modeling of optical nuclear polarization though delocalized electrons did suggest that this mechanism could contribute significantly to the observed nuclear polarizations, but delocalized electrons alone could not account for the experimental data.

The present results and analysis suggest that models limited to a single type of exited electron are overly simplistic. The data could be consistent with cross relaxation between nuclei and both localized and delocalized electrons. In terms of the relaxation-spin diffusion model, the data could be fit using alternative forms of $f(r)$ that include relaxation in the bulk [$\lim_{r\to\infty} f(r) > 0$]. This anticipated bulk relaxation could not be normal thermal relaxation because, for σ^+ light, bulk spins must relax towards the opposite polarization to thermal equilibrium. If multiple excited electrons are involved in optical nuclear polarization, it is also possible that $\langle I_z \rangle_\infty$ and $T_{1,0}$ are also spatially dependent. There is evidence in the literature that multiple types of electrons, with distinct g factors, participate in the optical nuclear polarization process.[3,21] Fur-

ther research is necessary to characterize the electron spin dynamics in semi-insulating GaAs.

As photon energy is increased above the band gap, it is reasonable to expect delocalized electrons to play a greater role in polarization of bulk nuclear spins. This expectation is born out in the lack of asymmetric quadrupolar line shapes observed for superband gap irradiation, i.e., comparison of signal intensities for optical pumping above and below the band gap indicates that superband gap irradiation results in lower polarizations for larger numbers of spins.

VI. CONCLUSION

By measuring bulk-averaged nuclear spin polarizations independently of the total NMR intensity, we have enabled further analysis of the origin of optical NMR enhancements. For irradiation below the band gap, our data revealed high nuclear spin polarizations and significant spatial inhomogeneity of electron-nuclear cross relaxation rates. The time dependences of signal intensity and nuclear spin polarization for irradiation at 1.505 eV have placed new constraints on the geometry of nuclear relaxation within the sample. Comparison of data to an equation for coupled nuclear spin relaxation and magnetization transport has revealed that sources of enhanced nuclear magnetization are neither completely localized to within the Bohr radii of trapped electrons, nor completely delocalized throughout the illuminated region. Results suggest that both localized and delocalized electrons could play a role in optical nuclear polarization. Irradiation above the band gap resulted in signal from larger numbers of spins with lower average polarizations, suggesting a more delocalized mechanism at higher photon energies.

ACKNOWLEDGMENTS

We are indebted to David Bindel for assisting with the Matlab code to solve Eq. (11). A.K.P. acknowledges support from the SEGRF program at the Lawrence Livermore National Laboratory for financial support.

APPENDIX A: ESTIMATES OF EXCITED ELECTRONIC SPIN POLARIZATION

The largest observed nuclear spin polarization in Fig. 2 ($\overline{\langle I_z\rangle}=-0.4$ after 30 s of irradiation with 1.505 eV light, σ^+ polarization) places bounds on the excited electronic spin polarization, $\langle S_z\rangle$. The two polarizations are related to one another by the Solomon equation for the Overhauser effect:[3,22,23]

$$\langle S_z\rangle = S_0 + \frac{S(S+1)}{I(I+1)}\frac{w_0 + 2w_{1,I} + w_2}{w_0 - w_2}(\langle I_z\rangle - I_0), \quad \text{(A1)}$$

where S and I are total spins of the electrons and nuclei, respectively ($1/2$ and $3/2$, respectively), w_0, $w_{1,I}$, and w_2 are the first-order rate constants for zero-, single (nucleus), and double-quantum transitions involving coupled electrons and nuclei, and I_0 is the (negligible) thermal equilibrium nuclear spin polarization. For an Overhauser effect induced solely by the Fermi contact interaction, the only nonzero rate constant would be w_0, and the quotient of rate constants in Eq. (A1) would be unity; if other rate constants are nonzero, this quotient can only increase. We use the published value of -0.44 for the electronic g factor[2,24] to estimate the thermal equilibrium electronic spin polarization at $S_0=0.136$ (sample temperature$=10$ K and $B_0=9.4$ T). As a result, we estimate $\langle S_z\rangle \leqslant 0.056$ for irradiation at 1.505 eV with σ^+ light. We stress that, since w_2 and $w_{1,i}$ maybe nonzero, this prediction is a bound on the minimum deviation of $\langle S_z\rangle$ from S_0.

Further analysis of the relaxation of excited electron spins allows prediction of the modulation of $\langle S_z\rangle$ for different light polarizations. The steady-state excited electron spin polarization is given by

$$\langle S_z\rangle = \frac{S_0 + \dfrac{T_{1e}}{\tau_e}S_e}{1 + \dfrac{T_{1e}}{\tau_e}}, \quad \text{(A2)}$$

where T_{1e}/τ_e is the ratio of electron spin lifetime to the decay time of the excited state, and S_e is the spin polarization of optically excited electrons.[7,25] For $\sigma_\pm$ light polarization, S_e is expected to be ∓ 0.25.[6,7] We therefore estimate that $T_{1e}/\tau_e \geqslant 0.26$ and $\langle S_z\rangle \geqslant 0.16$ for excitation with σ^- light.

Since the data in Fig. 2 are spatial averages and not representative of the local maximum $\langle I_z\rangle$, and w_2 is not expected to be negligible,[26] we anticipate that our calculations are underestimates of the true deviations of $\langle S_z\rangle$ from S_0. It would not be unreasonable to expect $\langle S_z\rangle$ to be significantly closer to its theoretical limits of ± 0.25.

[1] T. Pietrass, A. Bifone, T. Room, and E. L. Hahn, Phys. Rev. B **53**, 4428 (1996).
[2] P. L. Kuhns, A. Kleinhammes, T. Schmiedel, W. G. Moulton, P. Chabrier, S. Sloan, E. Hughes, and C. R. Bowers, Phys. Rev. B **55**, 7824 (1997).
[3] A. K. Paravastu, S. E. Hayes, B. E. Schwickert, L. N. Dinh, M. Balooch, and J. A. Reimer, Phys. Rev. B **69**, 075203 (2004).
[4] C. A. Michal and R. Tycko, Phys. Rev. B **60**, 8672 (1999).
[5] T. Pietrass and M. Tomaselli, Phys. Rev. B **59**, 1986 (1999).
[6] R. Tycko and J. A. Reimer, J. Phys. Chem. **100**, 13240 (1996).
[7] *Optical Orientation*, edited by F. Meier and B. P. Zakharchenya (Elsevier, Amsterdam, 1984).
[8] G. Lampel, Phys. Rev. Lett. **20**, 491 (1968).
[9] D. Paget, Phys. Rev. B **25**, 4444 (1982).
[10] C. R. Bowers, Solid State Nucl. Magn. Reson. **11**, 11 (1998).
[11] M. Eickhoff and D. Suter, J. Magn. Reson. **166**, 69 (2004).
[12] S. E. Barrett, R. Tycko, L. N. Pfeiffer, and K. W. West, Phys. Rev. Lett. **72**, 1368 (1994).
[13] P. T. Callaghan, *Principles of Nuclear Magnetic Resonance Microscopy* (Oxford Science, New York, 1991).

[14] E. Fukushima and S. B. Roeder, *Experimental Pulse NMR: A Nuts and Bolts Approach* (Perseus Books, Reading, MA, 1981).
[15] A. Abragam and M. Chapellier, Phys. Lett. **11**, 207 (1964).
[16] P. R. Bevington and D. K. Robinson, *Data Reduction and Error Analysis for the Physical Sciences* 2nd ed. (McGraw-Hill, New York, 1992).
[17] P. G. deGennes, J. Phys. Chem. Solids **7**, 345 (1958).
[18] N. Bloembergen, Physica (Amsterdam) **15**, 386 (1949).
[19] I. J. Lowe and D. Tse, Phys. Rev. **166**, 279 (1968).
[20] G. W. 't Hooft, W. A. J. A. van der Poel, L. W. Molenkamp, and C. T. Foxon, Phys. Rev. B **35**, 8281 (1987).
[21] A. Paravastu and J. Reimer (unpublished).
[22] I. Solomon, Phys. Rev. **99**, 559 (1955).
[23] A. Abragam, *Principles of Nulcear Magnetism* (Oxford University Press, New York, 1996).
[24] C. Weisbuch and C. Hermann, Phys. Rev. B **15**, 816 (1977).
[25] A. K. Paravastu, Ph.D. thesis, University of California Berkeley, 2004.
[26] R. Tycko, Mol. Phys. **95**, 1169 (1998).
[27] The dark spectrum was acquired immediately after cooling the sample to liquid helium temperatures. Subsequent to saturation of nuclear magnetization at 10 K, nuclear spin relaxation times were sufficiently long to prohibit observation of significant intensity without laser enhancement.
[28] It can be shown with Eq. (A1) that such large nuclear spin polarizations are possible in GaAs given the maximum electronic spin polarization of ±0.25.